

TESTING OF POST-TENSIONED CONCRETE GIRDERS WITH NO SHEAR REINFORCEMENT

By

GUSTAVO LLANOS, BRANDON E. ROSS,
MARCUS H. ANSLEY, AND H. R. (TREY) HAMILTON



Authorized reprint from: July 2012 issue of the PTI Journal

Copyrighted © 2012, Post-Tensioning Institute
All rights reserved.

TESTING OF POST-TENSIONED CONCRETE GIRDERS WITH NO SHEAR REINFORCEMENT

by Gustavo Llanos, Brandon E. Ross, Marcus H. Ansley, and H. R. (Trey) Hamilton

The shear capacity of an early (circa 1950s) concrete bridge girder design used in Florida was experimentally evaluated by testing three full-scale replica girders. The girders were simply supported, precast, post-tensioned (PT) I-girders with end blocks. Most notably, the original plans did not include shear reinforcement outside of the end blocks and specified direct concrete-on-concrete bearing conditions. Two girders were tested with a shear span-depth ratio (a/d) of 3.0 to compare a direct concrete bearing support condition with a neoprene bearing pad support condition. The failure mode of both of these girders was flexure. The third girder was tested with $a/d = 2.0$ to determine the shear capacity. Although loading was terminated prior to reaching capacity, the data indicate that the prestressing steel had yielded and a plastic hinge had formed. The peak shear in each girder well exceeded the predictions of both the ACI 318-08 detailed method and the modified compression field theory (MCFT). The bearing condition did not significantly affect shear capacity, but it did affect displacement capacity.

KEYWORDS

Bearing conditions; existing structure; historic post-tensioning; losses; shear capacity; shear reinforcement; strut-and-tie.

INTRODUCTION

Many early (circa 1950s) post-tensioned (PT) concrete girders are still in service in Florida. These girders are precast, PT I-girders with end blocks used in simply supported short-span bridges. Typically, they bear directly on concrete pier caps with only a layer of tar paper separating the two. These girders are of particular interest because they have both parabolic and straight PT bars, and

they have no shear reinforcement. Mild steel reinforcement was provided only at the end blocks for approximately 3 ft (914 mm) from each end.

The shear capacity of these early girders has been of concern due to the lack of shear reinforcement and the associated low shear capacity from rating calculations. To address this concern, three replica girders were constructed using original bridge plans and then tested in three-point bending to determine the girder shear capacity. Two of the girders were tested using a shear span-depth ratio (a/d) of 3.0. The final girder was tested using an a/d of 2.0.

The concrete-to-concrete bearing used for the early Florida girders is different from the current practice of using reinforced neoprene bearing pads at girder supports. Previous research has reported that bearing condition can affect the moment distribution in girders, thereby changing girder capacity and behavior.¹ To evaluate the effects of different bearing conditions, one of the girders tested at an a/d of 3.0 was supported directly on concrete, whereas the other girder tested at the same a/d was supported on neoprene bearing pads.

RESEARCH SIGNIFICANCE

This paper presents an experimental evaluation of the shear capacity of early PT girders that do not meet current code requirements for shear strength and reinforcement. The results are compared to current code models, including the detailed method of the American Concrete Institute (ACI) 318-08³ and AASHTO's modified compression field theory (MCFT),⁴ and the strut-and-tie method (STM). In addition, direct concrete bearing, which is likely to generate some arching action, is compared to bearing on a neoprene pad. Information in this paper will help engineers evaluate similar existing girders and bearing conditions.

GIRDER DESIGN

Three test girders were constructed using existing 1950s bridge plans. The nearly 47 ft (14.3 m) long test

PTI JOURNAL, V. 8, No. 1, July 2012. Received and reviewed under Institute journal publication policies. Copyright ©2012, Post-Tensioning Institute. All rights reserved, including the making of copies unless permission is obtained from the Post-Tensioning Institute. Pertinent discussion will be published in the next issue of *PTI JOURNAL* if received within 3 months of the publication.

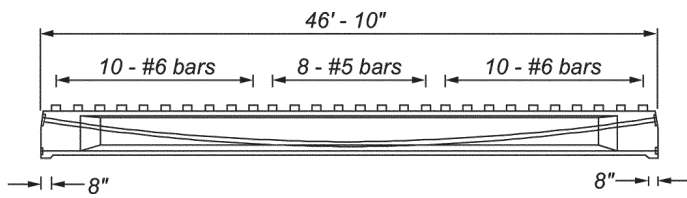


Fig. 1—Girder elevation. (Note: 1 ft = 304.8 mm; 1 in. = 25.4 mm.)

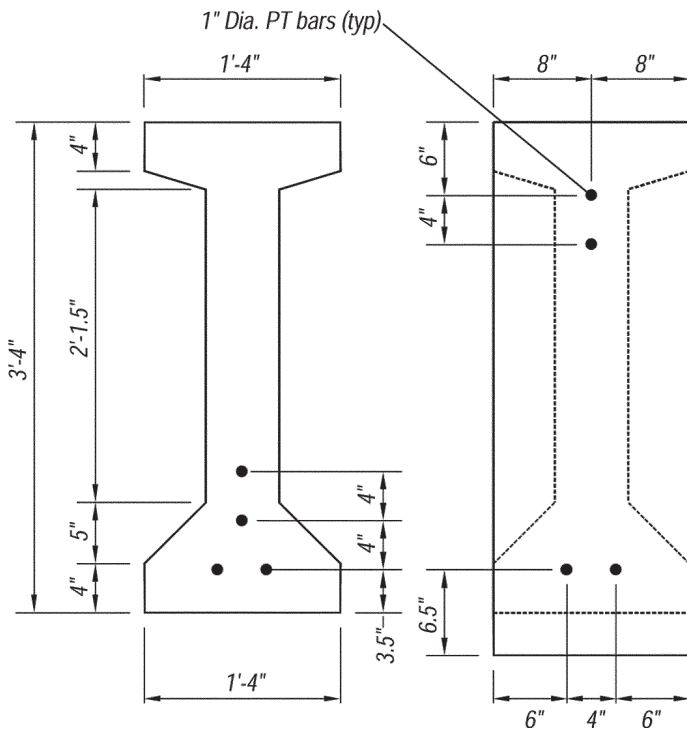


Fig. 2—Cross section and post-tensioning bars details at midspan (left) and end (right). (Note: 1 ft = 304.8 mm; 1 in. = 25.4 mm.)

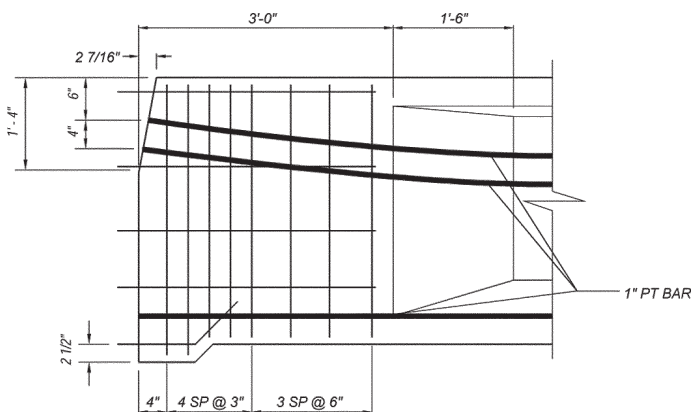


Fig. 3—End block geometry, reinforcement, and PT bar configuration. (Note: 1 ft = 304.8 mm; 1 in. = 25.4 mm.)

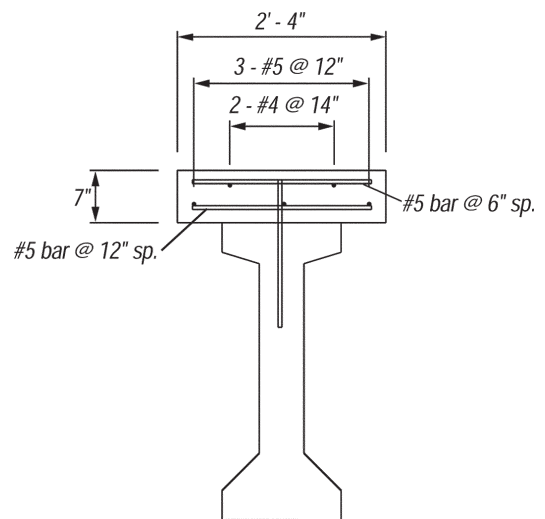


Fig. 4—Deck geometry and reinforcement. (Note: 1 ft = 304.8 mm; 1 in. = 25.4 mm.)

girders had four 1 in. (25.4 mm) diameter PT bars (Fig. 1). This was a slight alteration from the existing plans, which called for 1.125 in. (28.6 mm) diameter bars. The PT steel bars specified in the existing bridge plans were not available, so commercially available Grade 150 bars ($f_{pu} = 170$ ksi [1172 MPa]) were used to construct the test girders. Samples of the bars used in constructing the test girders were tested, showing an average tensile strength of 169.9 ksi (1171 MPa). As in the original girder plans, two PT bars were placed in a parabolic configuration with the other two PT bars placed at the bottom of the girder in a straight configuration (Fig. 2). Each bar had a cross-sectional area of 0.85 in.² (548 mm²). Mild steel was placed in the end block for 34 in. (864 mm) at each end of the girder (Fig. 3). The longitudinal steel in the end block extended just beyond the last stirrup. U-shaped bars were placed along the top of the girder to ensure composite action between the deck and the girder but did not extend a sufficient distance into the girder to provide additional shear capacity. A 2 ft 4 in. (711 mm) wide by 7 in. (178 mm) thick deck was cast on the girder to simulate the 7 in. (178 mm) thick bridge deck used in the original design (Fig. 4). The deck was reinforced with two layers of transverse No. 5 bars and longitudinal No. 4 bars.

GIRDER CONSTRUCTION

Test girders were constructed at the Florida Department of Transportation Structures Laboratory in Tallahassee, FL. Formwork was fabricated using welded steel panels, and the bottom form was placed on the top flange of a steel

I-beam, which served as a base during construction. After erecting one side of the formwork, mild steel cages (Fig. 5) were placed in the end block at each end of the girder. The cages were fastened to the formwork and rested on chairs to keep them in place while the concrete was placed. Each PT bar was placed in a separate 1.6 in. (40 mm) diameter galvanized steel duct. The ducts were fastened to the formwork and strapped to chairs at incremental points along the girder length to maintain the parabolic or straight configuration during casting. Plywood bulkheads were positioned to enclose the ends of the forms.

Anchorage bearing plates consisted of 1.75 x 6 x 10 in. (44.5 x 152 x 254 mm) steel plates with countersunk, conical-shaped holes. The PT bars were anchored with coarse threaded nuts that had dome-shaped ends that fit into the conical-shaped holes in the bearing plates. This system self-corrected to maintain bar alignment relative to the anchor plate during stressing. After installing bulkheads and anchorages at each end of the girder, tubes and vents necessary to facilitate grouting were installed along the length of the girder. Strain gauges were applied to the bars to monitor prestressing losses. U-bars were tied to a longitudinal bar placed near the top of the girder (Fig. 6). The opposite form was then installed with all-thread rods used as form ties.

The girders were cast using ready mixed concrete that was bucketed to the form using the laboratory crane. The water-cement ratio (w/c) was 0.41 and the aggregate was 3/4 in. (19 mm) Florida limestone. One truckload of concrete was needed for each girder. Cylinders were made for testing concrete compressive strength. PT bars were stressed after the cylinders' compressive strength reached 3600 psi (24.8 MPa) or greater, which was typically in 3 to 5 days. Table 1 lists the strength of the concrete corresponding to the day each girder was tested.

The PT ducts were grouted immediately after stressing using a portland cement and water mixture with a w/c of 0.45. Grout was injected from one end of the girder and was continuously pumped until the discharge at the opposite end indicated that air and water had been removed.

After grouting, the deck formwork and mild steel reinforcement were placed. As with the girder, concrete for the deck was delivered using the laboratory crane. A finished girder is shown in Fig. 7. Cylinders of the deck concrete were taken and tested, with results reported in Table 1.

PRESTRESSING

Prestressing application

A hydraulic jack was used to stress the PT bars (Fig. 8). This jack is an 80 ton (712 kN) hydraulic actuator designed



Fig. 5—End block reinforcement cage.



Fig. 6—U-bar positioning and form ties.

Table 1—Average cylinder strength

Girder	Girder, ksi (MPa)	Deck, ksi (MPa)
C1	7.96 (54.9)	3.34 (23.0)
C2	8.64 (59.6)	5.47 (37.7)
C3	8.64 (59.6)	4.89 (33.7)



Fig. 7—Finished girder and deck.



Fig. 8—Hydraulic jack used to stress PT bars.

to stress a single thread bar. The jack had an integral socket for tightening the PT nut prior to release. The target prestress force for each bar was 93 kips (414 kN) and was measured with a load cell placed between the PT nut and jack.

To avoid exceeding allowable concrete stresses, the bars were stressed in two stages in the following order: 2, 3, 1, and 4 (Fig. 9). The first stage consisted of stressing each PT bar to 50% of the desired final stress in the order indicated. The stressing sequence was then repeated to reach the final stress.

Instrumentation

Strain gauges were applied to the PT bars to measure prestress losses during and after stressing and stresses in the bars during load testing. Tandem gauges were placed on the bars near each end of the girder (Fig. 10). The gauges were placed in diametrically opposed positions on the bar to account for possible bending strain in the bar. Stresses

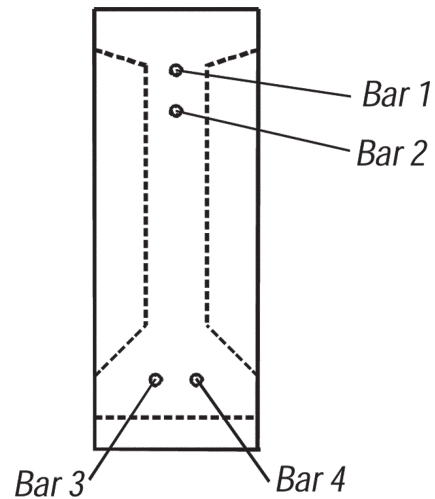


Fig. 9—PT bar designation.

were calculated by multiplying the measured strains by Young's modulus. Some of the gauges were damaged during installation and prestressing of the PT bars.

Results—losses

Measurements were taken during post-tensioning to determine anchorage set, elastic losses, friction losses, and early creep losses.

Anchorage set in prestressing bar anchorages occur when the bar is released and the anchor nut settles against the anchor plate. Further set occurs as the anchorage components deform during transfer. As the PT bar was being stressed, the anchor nut was tightened to minimize the take up when the bar was released.

Anchorage set can be measured by observing the change in strain as the prestress is transferred. Strain data from the gauges located nearest the stressing end of the girder will more accurately show anchorage set because the strain gauges at the dead end will be affected by friction losses from wobble or drape.

Figure 11 illustrates how elastic losses and anchorage set were determined from the strains measured in the bars during post-tensioning. As noted on the plot, anchorage set was the immediate reduction in stress as the prestress force was transferred from the jack to the anchorage. The three subsequent sharp drops in stress indicate the elastic losses caused by stressing each of the adjacent PT bars. The shallower downward trends indicate initial creep losses. Similar anchorage set, elastic losses, and creep behavior occurred at both stages of stressing.

Anchorage set losses are summarized in Fig. 12. Typically, the anchorage set losses were measured using

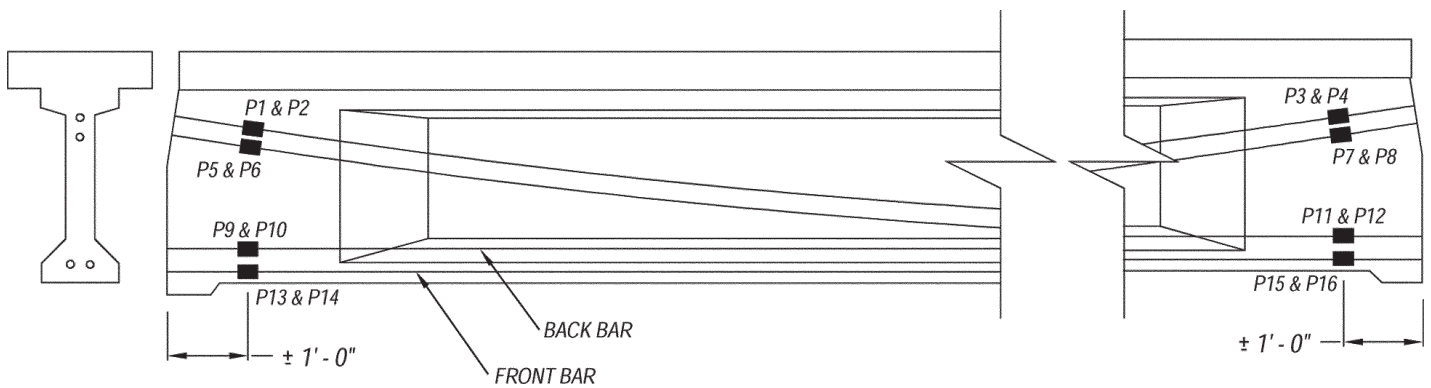


Fig. 10—Location of gauges for C girders. (Note: 1 ft = 304.8 mm; 1 in. = 25.4 mm.)

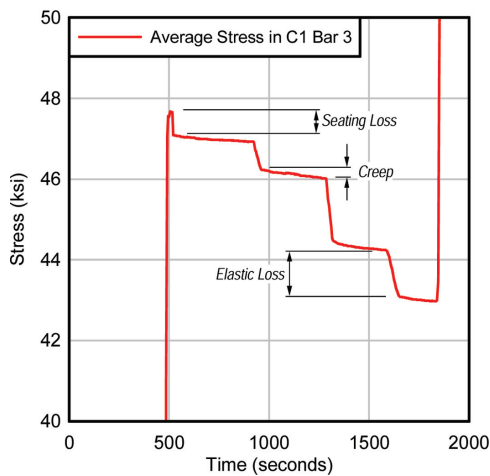


Fig. 11—Measurement of anchorage set, short-term creep, and elastic loss. (Note: 1 ksi = 6.9 MPa.)

strain gauges on the stressing end of the girder; however, due to the loss of gauges during construction, anchorage set losses for Bars 3 and 4 in Girder C2 were measured using the strain gauges at the dead end. Anchorage set losses for the straight PT bars (3 and 4) were consistently in the range of 2% regardless of the jacking stress. The parabolic PT bar, however, had anchorage set losses two to three times this value. This is likely due to the friction generated in the parabolic tendon along the curvature of the tendon.

The anchorage set at the stressing end anchorage was calculated using the initial change in strain due to seating loss (Fig. 12) and multiplying it by the length of the PT bars, 46 ft 10 in. (14.3 m). Results are presented in Table 2. Typical values of anchorage set have been reported to be approximately 0.03 in. (0.76 mm), but will vary depending on the type of anchorage.²

As shown in Fig. 11, the bars also experienced elastic losses as the other bars were stressed. In general, the highest

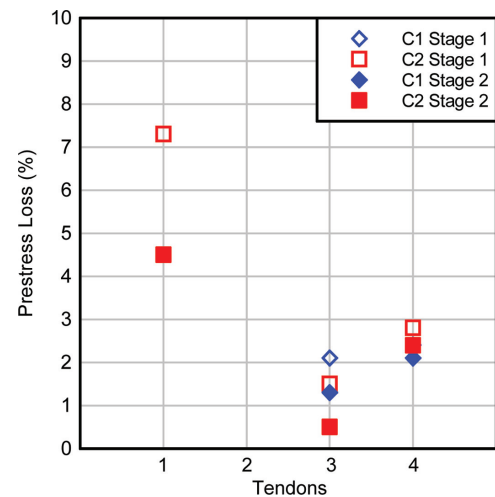


Fig. 12—Summary of anchorage set loss.

Table 2—Measured anchorage set in in. (mm)

PT Bar	Stage 1		Stage 2	
	C1	C2	C1	C2
1	—	0.06 (1.52)	—	0.09 (2.29)
3	0.02 (0.51)	0.02 (0.51)	0.02 (0.51)	0.01 (0.25)
4	0.03 (0.76)	0.03 (0.76)	0.04 (1.02)	0.05 (1.27)

losses were observed during the stressing (jacking) of immediately adjacent PT bars. Figure 13 gives a summary of the total elastic losses over both stages of stressing.

Wobble in a straight duct will generate friction, which will cause a reduction in the PT force as the distance from the jacking location increases. The wobble coefficient was calculated for PT Bar 4 in C1 by determining the difference between the bar stress (using the strain gauges) at the jacking

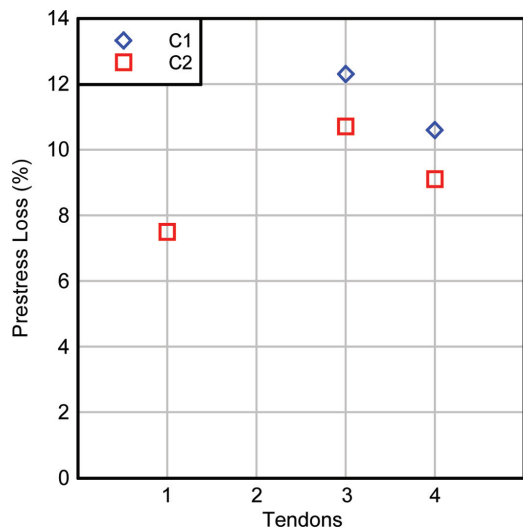


Fig. 13—Summary of elastic losses.

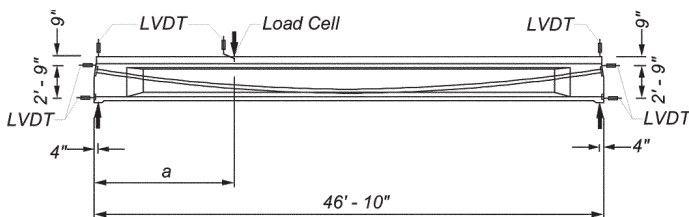


Fig. 14—Test setup and instrumentation.



Fig. 15—Support conditions: C1 (left); and C2 (right).

end and dead end of the PT bar. A wobble coefficient of 0.0007 per ft (0.21 per mm) was then back-calculated. ACI 318-08³ gives a range for the wobble coefficient of 0.0001 to 0.0006 per ft (0.03 to 0.18 per mm) for high-strength bars grouted in metal sheathing.

To observe time-dependent losses, PT stresses Bars 1 and 4 of C2 were measured for approximately 2.5 days after stressing. The losses due to creep and shrinkage effects were 6.3 and 5.6% for this short period of measurement. By comparison, a loss of 1.7% was obtained using the AASHTO LRFD⁴ method for calculating shrinkage and creep losses.

TEST SETUP AND PROCEDURES

Each girder was tested using a three-point loading scheme, as shown in Fig. 14. Girders C1 and C2 were tested using an a/d of 3.0. Girder C1 was supported directly on a concrete pedestal (Fig. 15). Girder C2 was set up with the girder bearing on 2 in. (51 mm) thick neoprene pads. Girder C3 was loaded at $a/d = 2.0$ and was supported on neoprene pads.

The load was applied by an actuator through a 1.5 x 10 x 20 in. (38 x 254 x 508 mm) thick (20 in. [508 mm] dimension perpendicular to length of girder) reinforced neoprene bearing pad at a loading rate of 0.25 kips/s (1.11 kN/s). For tests with neoprene bearing pads at the supports, the pad dimensions were 2 x 8 x 16 in. (51 x 203 x 406 mm) thick (16 in. [406 mm] dimension perpendicular to length of girder). A load cell was used to measure the load under the actuator. Using linear variable differential transformers (LVDTs), the vertical displacements were measured at the load point and at each of the supports. LVDTs were also used to measure the horizontal movement at the top and bottom of the girder (Fig. 14). Strain gauges were applied to strategic locations on the girder flanges, girder web, and deck.

RESULTS AND DISCUSSION—SHEAR TESTS

Tests C1 and C2, $a/d = 3$

As previously mentioned, the bearing conditions varied for the two tests conducted at an a/d of 3.0. Girder C1 was supported directly on concrete and Girder C2 was supported on neoprene pads. Figure 16 shows the superimposed shear-versus-displacement plot for both girders. The initial elastic behavior of both girders was similar, as was the shear load at initial cracking. Strain gauges from both tests confirmed initial cracking at a shear of 74 kips (329 kN). Figure 17 shows the initial and final crack patterns for Girders C1 and C2.

For Girder C1, the initial flexural crack was followed by further flexure cracks and a decrease in stiffness. The girder reached a maximum shear load of 135 kips (601 kN), where a flexure-compression failure occurred in the deck under the load point.

Girder C2 displayed a different post-cracking behavior than C1. The stiffness of C2 began decreasing when the shear load reached approximately 92 kips (409 kN), as indicated by the decrease in the slope of the load displacement curve (Fig. 16). As loading continued, the curve eventually reached a plateau, indicating yielding of the PT bars. The girder reached its maximum capacity at a

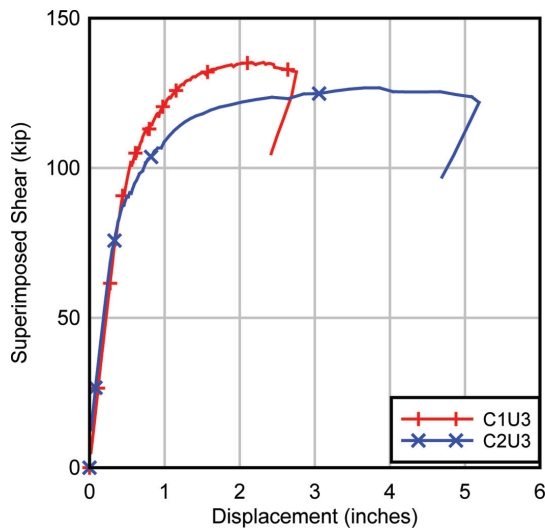


Fig. 16—Superimposed shear-versus-displacement for C1. (Note: 1 kip = 4.5 kN; 1 in. = 25.4 mm.)

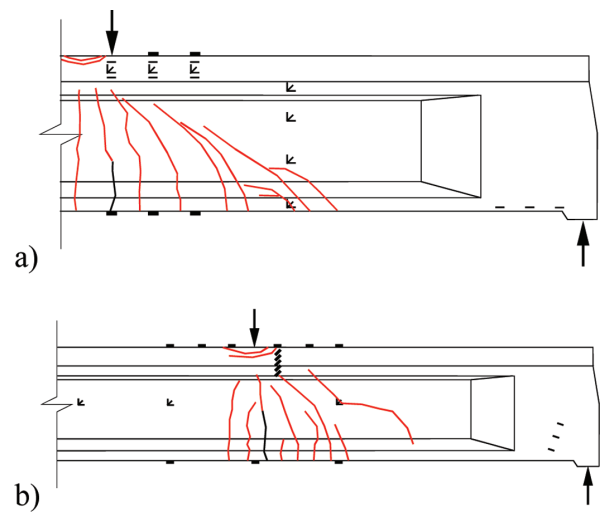


Fig. 17—Crack patterns: (a) C1; and (b) C2 (initial cracks in black).

shear of 127 kips (565 kN), where a flexure-compression failure occurred in the deck under the load point.

Test C3, $a/d = 2$

Figure 18 shows the superimposed shear-versus-displacement plot for Test C3. The plot indicates linear elastic behavior up to a shear of 87 kips (387 kN). The initial crack (Fig. 19) was visually observed at this load and was confirmed by strain-gauge data. Strain-gauge data also confirmed the formation of additional cracks at 109 and 153 kips (485 and 681 kN). The shear displacement curve (Fig. 18) shows a reduction in stiffness over this same range of loads. The crack that formed at a shear of 156 kips (694 kN) was observed to extend from the tension face below the end block up into the web (Fig. 20). The shear displacement curve had reached a plateau at a displacement of 1.5 in. (38 mm) with little increase in shear relative to displacement, indicating that the PT bars had yielded.

Cracks were observed around the anchor plate of the parabolic PT bars at a shear of 187 kips (832 kN). The test was terminated at this point to avoid an explosive failure. The final crack pattern can be seen in Fig. 19. The peak shear force during testing was 187 kips (832 kN). The final failure mode, however, was not determined because the test was terminated prior to failure.

EFFECT OF SUPPORT CONDITIONS ON BEHAVIOR

Tests C1 and C2 were conducted with an a/d of 3.0. The first test, C1, used the support conditions shown in

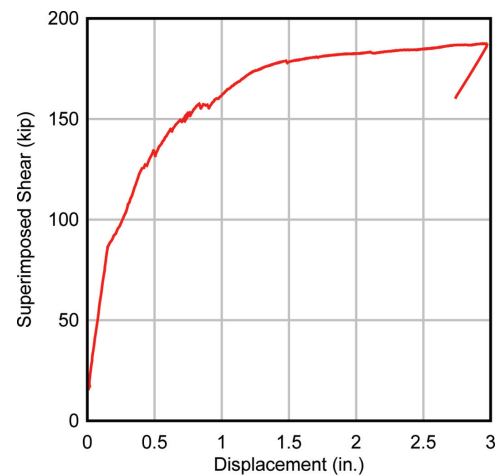


Fig. 18—Superimposed shear-versus-displacement for C3. (Note: 1 kip = 4.5 kN; 1 in. = 25.4 mm.)

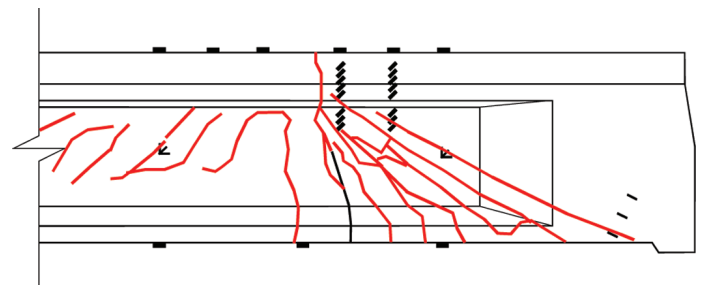


Fig. 19—Crack pattern for C3 (initial crack in black).

Fig. 21, where the girder was bearing directly on concrete. The second test, C2, used neoprene pads under each of the supports (Fig. 22). Both tests had the same loading scheme and loading rate; the support conditions were the only variable between the two tests. The intent of the test was to explore the difference in behavior between the two support conditions.

The overall behavior of Tests C1 and C2 are illustrated in Fig. 16. As discussed previously, the shear at which cracking occurred was approximately 74 kips (329 kN) for both tests. Furthermore, the behavior up to cracking

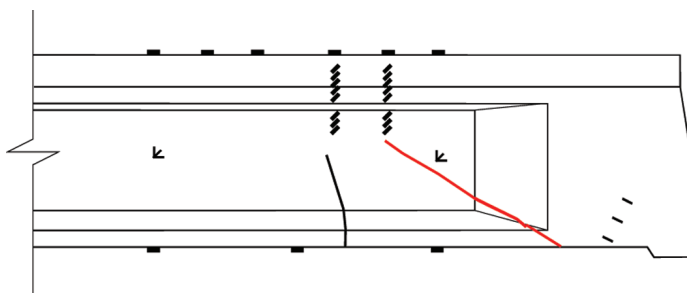


Fig. 20—First crack (black) and crack occurring at 156 kips (694 kN) (red).

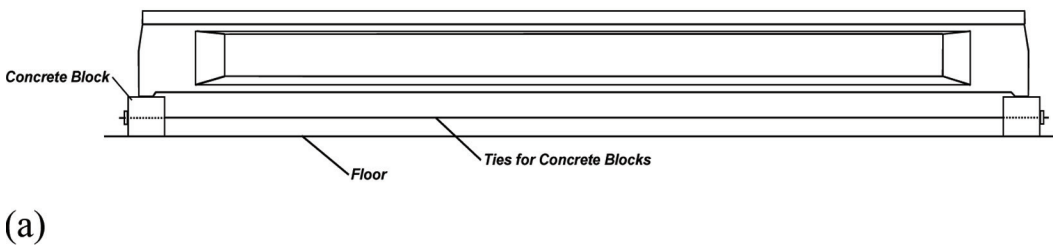


Fig. 21—Support condition for C1.

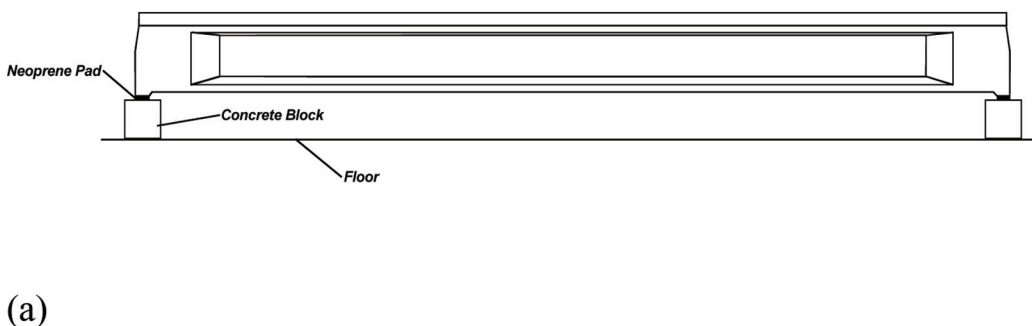


Fig. 22—Support condition for C2.

appears similar between the two girders, indicating that the different support conditions had little effect before the girder cracked. This lack of difference is likely due to the relatively small amount of support movement needed to relieve arching action before cracking occurs.

Figure 23 shows the flexural tensile strain under the load point and the total lateral displacement of the girder bearing. Note that the total lateral displacement is the sum of the displacement measured at both ends of the girder and was nearly identical for each girder up to cracking. The total movement measured for C1 and C2 at a superimposed shear of 70 kips (311 kN) was 0.080 and 0.085 in. (2.0 and 2.2 mm), respectively.

For the direct concrete bearing condition, it is suspected that support blocks adjusted slightly as load was applied, relieving the arching action prior to cracking. As for the neoprene bearing condition, the movement at the supports was so small that it generated little transverse reaction. Thus, the bearing conditions used in these tests appear to have had little effect on the behavior of the girders under service level loads (before cracking). This behavior is expected from girders in the field with similar bearing conditions.

However, the behaviors began to diverge at loads beyond cracking (Fig. 18). The direct bearing test, C1, had a higher post-cracking stiffness and had a 6.8% higher capacity than that of the neoprene bearing test, C2. The ultimate displacement, however, was approximately 59.0% of the neoprene bearing test.

Evidence of post-cracking bearing restraint is seen in the divergence of lateral displacements as ultimate capacity is approached (Fig. 23). After cracking, the total outward support movement of the neoprene bearing test, C2, was greater than that of the direct bearing test, C1, indicating that the transverse force generated at the support for C1 was beginning to affect the behavior. This difference is an indication that the frictional force generated by the direct concrete bearing was greater than that provided by the neoprene bearing pads. In conclusion, the direct contact bearing provided more restraint than that of the neoprene bearing pad, resulting in higher capacity but less ductility.

COMPARISON WITH THEORETICAL CAPACITIES

Table 3 shows a comparison of the experimental girder capacity with calculated capacities using the following methods:

1. MCFT from AASHTO LRFD Bridge Design Specification (2007)⁴;
2. STM from AASHTO LRFD Bridge Design Specification (2007)⁴; and
3. Detailed method from ACI 318-08.³

Nominal moment capacity M_n was calculated using the method of strain compatibility (Table 4). Material properties used in the moment, shear, and STM calculations were taken from the concrete cylinder and PT bar test data as follows: 4.0 ksi (27.6 MPa) compressive strength of concrete topping slab, 8.1 ksi (55.8 MPa) compressive strength of the concrete girder, 170 ksi (1172 MPa) ultimate strength of PT bars, and 29,700 ksi (204.8 GPa) Young’s modulus of PT bars. The concrete compressive strengths are representative of the range of tested values. A Ramberg-Osgood equation was fit to the stress-strain curve for use in the strain compatibility calculations. Based on the experimental data, 11% was used for the initial losses.

Based on the AASHTO⁴ equation, 33% was used for the long-term losses.

Data gathered and observations made during testing indicate that the girders had reached (or nearly reached) their flexural capacity. This is corroborated by the large difference between the tested capacity and calculated shear capacities. Consequently, the experimental capacities shown in Table 3 provide a lower-bound strength for comparison with the calculated shear strengths.

The STM procedure was applied only to Girder C3 ($a/d = 2$). Figure 24 shows the strain profile for this girder. As indicated by the strain profile, Girder C3 ceased flexural behavior and commenced strut-and-tie behavior with the formation of a crack at a shear of 153 kip (681 kN). The STM in Fig. 25 shows the internal forces in the girder at capacity. Based on the load-displacement curve, it is thought that the PT bars had reached yield before loading was terminated, which simplified determining the force in the bars. Consequently, it was assumed that the PT bars controlled the capacity rather than the nodal regions and struts. This assumption established the force in the PT bars at yield or beyond, and a stress of 170 ksi (1172 MPa) was used in the bars for the STM. Knowing the forces in the bars, the applied loads, and the reaction at the support, the

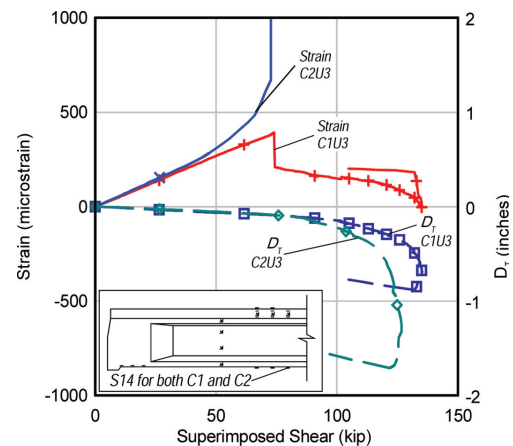


Fig. 23—Plot of tensile strain and total lateral displacement for C1 and C2. (Note: 1 kip = 4.5 kN.)

Table 3—Comparison of calculated shear capacity with experimental results

Test, a/d	V_{EXP} , kip (kN)	ACI		STM		MCFT	
		V_n , kip (kN)	V_{EXP}/V_n	V_n , kip (kN)	V_{EXP}/V_n	V_n , kip (kN)	V_{EXP}/V_n
C3, 2.0	196 (872)	92 (409)	2.13	213 (947)	0.92	111 (494)	1.77
C1, 3.0	142 (632)	66 (294)	2.15	—	—	93 (414)	1.53
C2, 3.0	133 (592)	66 (294)	2.02	—	—	93 (414)	1.43

Table 4—Post-tensioned girder nominal moment capacities

Test	a/d	M_{EXP} kip-ft (kN-m)	M_n kip-ft (kN-m)	M_{EXP}/M_n
C3	2.0	1507 (2043)	1402 (1901)	1.07
C1	3.0	1685 (2285)	1503 (2038)	1.12
C2	3.0	1587 (2152)	1503 (2038)	1.06

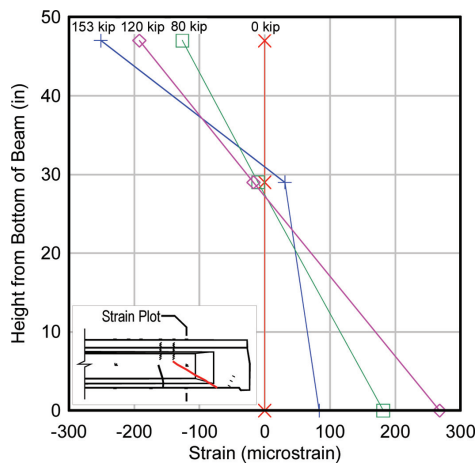


Fig. 24—C3 strain profiles. (Note: 1 kip = 4.5 kN; 1 in. = 25.4 mm.)

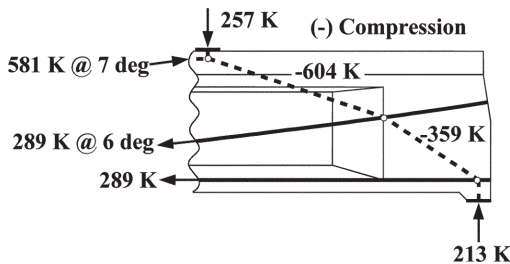


Fig. 25—Strut-and-tie model.

forces in the struts were found using a truss analysis. The STM gave the most accurate prediction of shear capacity, overestimating the capacity by approximately 8%. This is not surprising, however, because as with the flexural capacity, the bars controlled the shear capacity.

SUMMARY AND CONCLUSIONS

Three post-tensioned girders were constructed, closely matching a girder design used in Florida in the 1950s and tested. The girders had no shear reinforcement outside of the end block approximately 3 ft (914 mm) from each end of the girder. Each girder had two straight PT bars and two parabolic PT bars. The bars were placed in galvanized metal ducts and grouted.

During post-tensioning, the tendon stresses were monitored. Losses were calculated using strains and loads measured during stressing. Seating and elastic losses were determined from measured strain data. In addition, creep and shrinkage losses were monitored for approximately 2.5 days.

Two of the girders (C1 and C2) were tested with $a/d = 3.0$ to compare a direct concrete bearing support condition with a neoprene bearing pad support condition. The failure mode of both of these girders was flexure. The third girder (C3) was tested with $a/d = 2.0$ to determine the shear capacity. The loading was terminated prior to reaching peak capacity due to safety reasons. The experimental shear capacities were compared to the capacities predicted by MCFT,⁴ ACI,³ and STM⁴; and the experimental moment capacities were compared to the capacities predicted by the strain compatibility method.

Following are the salient findings from the research:

1. Girders bearing directly on concrete behaved the same as girders bearing on neoprene pads up until cracking occurred. The girder bearing directly on concrete displayed a 7% larger capacity than the girder bearing on a neoprene pad. The girder bearing on neoprene, however, attained nearly twice the displacement capacity than that of the girder bearing directly on concrete.

2. The failure mode of the $a/d = 2.0$ girders was flexure. The moment capacity of each girder was accurately predicted using the principles of strain compatibility. The calculated moment capacities using strain compatibility were between 6 and 12% lower than the experimentally determined capacities.

3. The failure mode of the $a/d = 3.0$ girders was not determined. The long and relatively flat load-deflection plot, however, indicates that the prestressing steel had yielded and that a plastic hinge had formed. The capacity predicted by both STM and strain compatibility were within 8% of the peak measured load. These two methods gave similar results because yielding of the prestressing steel controls the STM capacity.

4. None of the test girders failed in shear, even with the absence of shear reinforcement. The shear capacities calculated using both the design method³ and MCFT⁴ were well below the actual as-tested girder capacity in all three tests. ACI's³ experimental-to-calculated ratio ranged from 2.03 to 2.15, whereas MCFT's ratio⁴ was between 1.43 and 1.77. STM⁴ provided the closest capacity estimate at 0.92.

5. The average anchorage set loss for the straight tendons was approximately 2%. This translated to an anchorage set of 0.02 to 0.03 in. (0.51 to 0.76 mm). The

wobble coefficient for one of the straight tendons was 0.0007 per ft (0.21 per mm).

ACKNOWLEDGMENTS

The authors would like to acknowledge and thank the Florida Department of Transportation (FDOT) for funding this research project. In addition, the authors would like to thank D. Allen, F. Cobb, S. Eudy, T. Hobbs, W. Potter, P. Tighe, and C. Weigly of the FDOT Structures Research Center in Tallahassee, FL, for their assistance with the design, fabrication, and testing of these girders.

REFERENCES

1. Bakht, B., and Jaeger, L., "Bearing Restraint in Slab-on-Girder Bridges," *Journal of Structural Engineering*, ASCE, V. 114, No. 12, Dec. 1988, pp. 2724-2740.
2. Lin, T. Y., and Burns, N. H., *Design of Prestressed Concrete Structures*, John Wiley & Sons, 1981, 656 pp.
3. ACI Committee 318, "Building Code Requirements for Structural Concrete (ACI 318-08) and Commentary," American Concrete Institute, Farmington Hills, MI, 2008, 473 pp.
4. AASHTO LRFD Bridge Design Specifications, American Association of State Highway Transportation Officials, Washington, DC, 2007, 1512 pp.

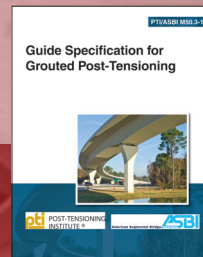
NOTATION

- a = distance from load point to nearest support
- d = average depth of longitudinal tensile reinforcement

- V_{EXP} = maximum experimental shear including superimposed shear and self-weight
- V_n = nominal shear capacity
- M_{EXP} = maximum experimental shear including super-imposed load and self-weight
- M_n = nominal moment capacity



NEW PTI BRIDGE PUBLICATIONS



PTI/ASBI M50.3-12, Guide Specification for Grouted Post-Tensioning

PTI M55.1-12, Specification for Grouting of Post-Tensioned Structures



PTI DC45.1-12, Recommendations for Stay Cable Design, Testing, and Installation

TO ORDER OR FOR MORE INFORMATION, VISIT THE BOOKSTORE AT WWW.POST-TENSIONING.ORG.

Gustavo Llanos is a Structural Engineer for BCC Engineering, Inc., in Miami, FL.

Brandon E. Ross, PE, is a Doctoral Student in the Department of Civil and Coastal Engineering at the University of Florida, Gainesville, FL.

Marcus H. Ansley, PE, is Director of the Florida Department of Transportation Structures Research Center in Tallahassee, FL.

H. R. (Trey) Hamilton, PhD, PE, is an Associate Professor of Civil and Coastal Engineering at the University of Florida, Gainesville, FL.